heating for an electron-attracting anode sheath is significantly higher than for an electron-repelling sheath, as would be expected from the higher current density. Defining an effective sheath potential as $\phi_{\text{eff}} \equiv q_e/j$ gives a similar value for the electron-repelling and electron-attracting sheaths in this experiment of $\phi_{\text{eff}} \sim 6.2 \pm 0.3$ V.

Langmuir probe measurements of an arcjet anode sheath show that the sheath potential drop can be of order 1–3 V positive or negative. The data suggest that the most significant factor in determining the sign of the potential is the anode current density, implying a critical current density for which $\phi_s = 0$. Here, $j_{\text{crit}} \sim 1$ A/cm^2.

In summary, a simple method of implementing langmuir probes has been presented that can provide direct measurements of n_{es}, T_{es}, j, and ϕ_s. Of the three methods outlined, determining ϕ_s from the plasma potential is the most reliable, since it is based on a direct measurement. Finally, as current density varies, the sheath voltage can change sign, and the arcjet anode heating can be represented by an effective potential $\phi_{\text{eff}} \sim 6.2$ V at the probe location used.

Acknowledgments

We gratefully acknowledge illuminating discussions with H. Krier and M. Kushner and critical assistance from W. Johnson, K. Elam, and J. Frizzell of the University of Illinois; support from T. Haag and J. Sankovic of NASA Lewis Research Center; Graduate Students S. Bufton and G. Willmes for assistance in the laboratory; and helpful suggestions from M. Cappelli of Stanford University. The authors acknowledge support by the U.S. Air Force Office of Scientific Research under Contracts F49620-92-J-0448 and -0280. Mitat Birkan is the Program Monitor.

References

[1]Lichon, P., and Sankovic, J., "Development and Demonstration of a 600 Second Mission Average Arcjet," 23rd International Electric Propulsion Conf., Paper 93-087, Sept. 1993.

[2]Meeks, E., and Cappelli, M. A., "A Multi-Fluid Model of Near-Electrode Plasma Behavior," AIAA Paper 93-2103, June 1993.

[3]Merinov, N. S., and Petrosov, V. A., "Existence Region for Arcing Conditions with Negative Anode Potential Drop," *Journal of Applied Mechanics and Technical Physics*, Vol. 17, No. 1, 1976, pp. 12–18.

[4]Diamant, K. D., private communication, Princeton Univ., Princeton, NJ, Oct. 1995.

[5]Oberth, R. C., "Anode Phenomena in High-Current Discharges," Ph.D. Dissertation, Dept. of Mechanical and Aerospace Engineering, Princeton Univ., Princeton, NJ, 1970.

[6]Goodfellow, K. D., and Polk, J. E., "Experimental Verification of a High-Current Cathode Thermal Model," AIAA Paper 95-3062, July 1995.

[7]Vainberg, L. I., Lyubimov, G. A., and Smolin, G. G., "High-Current Discharge Effects and Anode Damage in an End-Fire Plasma Accelerator," *Soviet Physics—Technical Physics*, Vol. 23, No. 4, 1978, pp. 439–443.

[8]Dinulescu, H. A., and Pfender, E., "Analysis of the Anode Boundary Layer of High Intensity Arcs," *Journal of Applied Physics*, Vol. 51, No. 6, 1980, pp. 3149–3157.

[9]Cappelli, M. A., "Modeling of the Near-Electrode Regions of Arcjets I: Coupling of the Flowfield to the Non-Equilibrium Boundary Layer," AIAA Paper 92-3109, July 1992.

[10]Soulas, G. C., and Myers, R. M., "Mechanisms of Anode Power Deposition in a Low Pressure Free Burning Arc," 23rd International Electric Propulsion Conf., NASA CR 194442, International Electric Propulsion Conf., Paper 93-194, Sept. 1993.

[11]Carney, L. M., and Keith, T. G., "Langmuir Probe Measurements of an Arcjet Exhaust," *Journal of Propulsion and Power*, Vol. 5, No. 3, 1989, pp. 287–293.

[12]Curran, F. M., and Haag, T. W., "An Extended Life and Performance Test of a Low Power Arcjet," AIAA Paper 88-3106, July 1988.

[13]Schott, L., "Electric Probes," *Plasma Diagnostics*, edited by W. Lochte-Holtgreven, Wiley, New York, 1968, pp. 668–731.

Application of the k-ω Turbulence Model to Quasi-Three-Dimensional Turbomachinery Flows

Rodrick V. Chima*
NASA Lewis Research Center, Cleveland, Ohio 44135

Introduction

MANY computational fluid dynamics codes for turbomachinery use the Baldwin–Lomax (B–L) turbulence model.[1] It is easy to implement in two dimensions and works well for predicting overall turbomachinery performance. However, it is awkward to implement in three dimensions, often has difficulty finding the length scale, has a crude transition model, and neglects freestream turbulence, surface roughness, and mass injection.

The k-ω model developed by Wilcox[2] is an appealing alternative for several reasons. First, it is the only two-equation model that can be integrated to the wall without requiring damping functions or the distance to the wall, and hence, should behave well numerically. Second, the effects of freestream turbulence, surface roughness, and mass injection are easily included in the model. Finally, transition can be simulated using the low Reynolds number version of the model.[3]

Menter applied the k-ω model to external flows and showed very good results for flows with adverse pressure gradients.[4] Liu and Zheng[5] described their implementation of the k-ω model in a cascade code that included an area change term to account for endwall convergence. They validated the model for a flat plate, and compared the B–L and k-ω models to measured surface pressures for a low-pressure turbine cascade. Since they did not use the low Reynolds number version of the model, their results showed problems resulting from early transition.

In this Note the low Reynolds number k-ω model was incorporated in the author's quasi-three-dimensional turbomachinery analysis code.[6] The code includes the effects of rotation, radius change, and stream-surface thickness variation, and also includes the B–L turbulence model. The k-ω model was implemented using many of Menter's[4] recommendations and an implicit approximate-factorization scheme described by Baldwin and Barth.[7] The model was tested for a transonic compressor with rotation and variable stream-surface radius and height, and for a transonic turbine vane with transition and heat transfer. Results were compared to the B–L model and to experimental data.

Quasi-Three-Dimensional Navier–Stokes Code

The quasi-three-dimensional Navier–Stokes equations have been developed for an axisymmetric stream surface in an (m, θ) coordinate system as shown in Fig. 1. The meridional coordinate m is given by $dm^2 = dz^2 + dr^2$, and the tangential coordinate θ rotates with the blade row with angular velocity Θ. The radius r and the thickness h of the stream surface are assumed to be known functions of m. The equations were mapped to a body-fitted coordinate system, nondimensional-

Received Nov. 27, 1995; presented as Paper 96-0248 at the AIAA 34th Aerospace Sciences Meeting and Exhibit, Reno, NV, Jan. 15–19, 1996; revision received May 27, 1996; accepted for publication May 28, 1996.

*Aerospace Engineer, M/S 77-6, Brookpark Road. Associate Fellow AIAA.

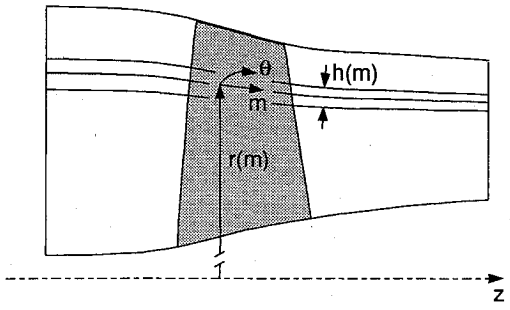

Fig. 1 Quasi-three-dimensional stream surface for a compressor rotor.

ized, and simplified using the thin-layer approximation. The flow equations and details of the explicit Runge–Kutta scheme are given in Ref. 6.

k-ω Turbulence Model

The k-ω turbulence model solves two transport equations for the turbulent kinetic energy k and the specific dissipation rate ω. A basic formulation is for fully turbulent flows and a low Reynolds number formulation is used for transition.[3] The quasi-three-dimensional form of the low Reynolds number k-ω equations is as follows:

$$\partial_t q + U\partial_\xi q + V\partial_\eta q - \frac{J}{\rho Re} G = \frac{1}{\rho}(P - D) \tag{1}$$

$$q = [k,\ \omega]^T \tag{2}$$

$$\mu_T = \alpha^*(\rho k/\omega) \tag{3}$$

The r and h appear in the θ metrics and the Jacobian, and Θ appears in the relative contravariant velocities U and V:

$$\begin{bmatrix} \xi_m & \xi_\theta \\ \eta_m & \eta_\theta \end{bmatrix} = J \begin{bmatrix} \theta_\eta & -m_\eta/r \\ -\theta_\xi & m_\xi/r \end{bmatrix} \tag{4}$$

$$J = [rh(m_\xi\theta_\eta - m_\eta\theta_\xi)]^{-1}$$

$$U = \xi_m u + \xi_\theta(v - r\Theta)$$

$$V = \eta_m u + \eta_\theta(v - r\Theta) \tag{5}$$

The diffusive terms G use the thin-layer approximation:

$$G = \frac{(\eta_m^2 + \eta_\theta^2)}{J} \begin{bmatrix} (\mu + \sigma^*\mu_T)\partial_\eta k \\ (\mu + \sigma\mu_T)\partial_\eta \omega \end{bmatrix} \tag{6}$$

The production terms P use the vorticity Ω as suggested by Menter[4]:

$$\frac{P}{\rho} = \begin{bmatrix} \dfrac{\mu_T}{\rho Re}\Omega^2 - \dfrac{2}{3}k\left(\partial_m u + \dfrac{1}{r}\partial_\theta v\right) \\ \alpha\left[\alpha^*\Omega^2 - \dfrac{2}{3}\omega\left(\partial_m u + \dfrac{1}{r}\partial_\theta v\right)\right] \end{bmatrix} \tag{7}$$

$$\Omega = \partial_m v - \frac{1}{r}\partial_\theta u + \frac{v}{r}d_m r$$

The destruction terms D are given by

$$\frac{D}{\rho} = \begin{bmatrix} \beta^*\omega k \\ \beta\omega^2 \end{bmatrix} \tag{8}$$

The baseline k-ω model has five coefficients, $\beta = 3/40$, $\beta^* = 9/100$, $\sigma = 1/2$, $\sigma^* = 1/2$, and $\alpha = 5/9$, and the trivial constant $\alpha^* = 1$. The low Reynolds number model replaces three of the constants with $\beta^* = (9/100)F_\beta$, $\alpha = (5/9)(F_\alpha/F_\mu)$, and $\alpha^* = F_\mu$, where F_i are the following bilinear functions of the turbulence Reynolds number Re_T:

$$F_\beta = \frac{5/18 + (Re_T/R_\beta)^4}{1 + (Re_T/R_\beta)^4}$$

$$F_\alpha = \frac{\alpha_0 + Re_T/R_\omega}{1 + Re_T/R_\omega} \tag{9}$$

$$F_\mu = \frac{\alpha_0^* + Re_T/R_k}{1 + Re_T/R_k}$$

$$Re_T = \frac{\rho k}{\mu_L \omega}$$

with $\alpha_0 = 1/10$, $\alpha_0^* = \beta/3 = 1/40$, and $R_\beta = 8$, $R_\omega = 27/10$, $R_k = 6$.

Boundary Conditions

At the inlet the turbulence intensity Tu and turbulent viscosity μ_T were specified. Then ω was found from Eq. (3) and k was found from

$$k = \tfrac{3}{2}Tu^2 U_{\text{in}}^2 \tag{10}$$

On solid walls $k = 0$, and ω was set using Wilcox's roughness model:

$$\omega_{\text{wall}} = \frac{\mu_\tau^2}{\nu} \times \begin{bmatrix} \left(\dfrac{50}{k_R^+}\right)^2 & k_R^+ < 25 \\ \dfrac{100}{k_R} & k_R^+ \geq 25 \end{bmatrix} \tag{11}$$

The equivalent sand grain roughness height k_R^+ was set to five, giving a hydraulically smooth surface.

Values of k and ω were extrapolated at the exit and treated as periodic across trailing-edge wake cut lines and between blade rows.

Approximate Factorization Solution Scheme

An implicit approximate–factorization scheme, described by Baldwin and Barth,[7] was used to solve the k-ω equations. Advective terms were approximated using first-order upwind differences and diffusive terms were approximated by second-order central differences. The destruction terms were linearized as suggested by Menter[4] and were included in the streamwise ξ factor. The production terms were treated explicitly. The k and ω equations were solved uncoupled from each other and from the flow equations.

The CPU time for one iteration of the k-ω model was only 5% more than that for one application of the B–L model. Experience has shown that it is sufficient to update the B–L model every five iterations. In general, it was necessary to update the k-ω model every two iterations with twice the time step of the flow solution, making a k-ω solution about 18% slower than a B–L solution.

Transonic Compressor Rotor Wake

The transonic compressor rotor studied by Suder et al.[8] was used to test the quasi-three-dimensional effects in the model. This rotor was used for a three-dimensional blind test case for turbomachinery codes organized by ASME and the International Gas Turbine Institute. Many of the codes used for the test case were unable to predict the measured wake spreading and decay. It was conjectured that the B–L model was re-

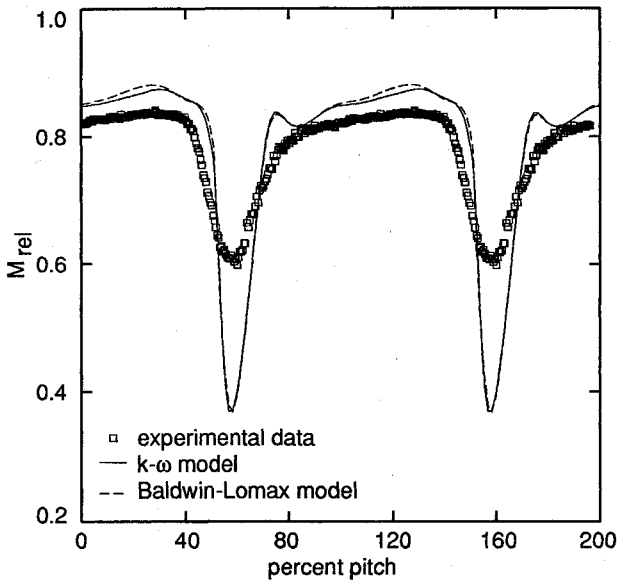

Fig. 2 Computed and measured near-wake Mach number profiles for a transonic compressor rotor.

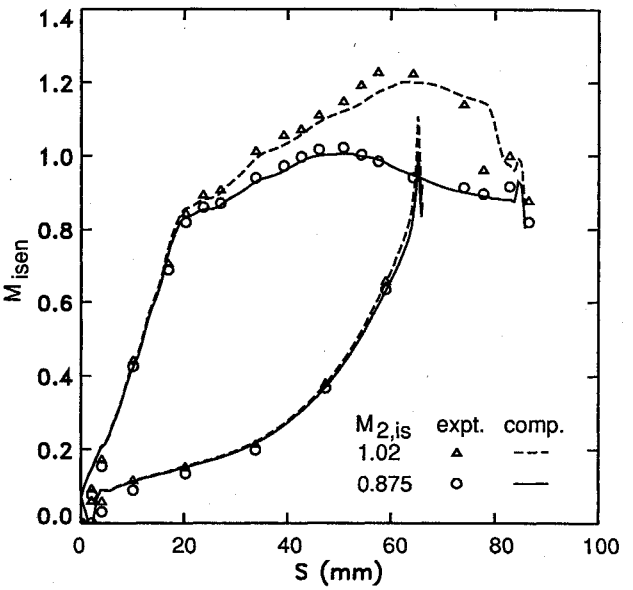

Fig. 3 Computed and measured distributions of isentropic Mach number for the von Kármán Institute turbine vane.

sponsible for the poor predictions and hoped that the k-ω model would improve the results.

A section of the rotor at 70% span was analyzed. The stream-surface r and h were specified to model the converging endwalls. The radius was specified as a line at 70% of local span, and h was specified as the local span normalized by the inlet span. A meridional view of the stream surface is shown in Fig. 1. The choice of r and h can have a first-order effect on the solution. However, the algebraic guess used here often gives reasonable results that can be used to compare turbulence models to each other.

A C-type grid with 319 × 45 points and a wall spacing of $y^+ < 2$ was used. The calculations were run 2000 iterations, which took about 3.25 min for the k-ω model on a Cray C-90 computer.

Figure 2 compares computed and measured Mach number profiles 0.28 chords downstream of the trailing edge. The k-ω (solid line) and B–L (dashed) results are nearly identical. The computed Mach number in the core flow is slightly high as a result of the specified stream surface, and the computed wakes are narrower and deeper than the measured wakes. Varying ω_{in} by five orders of magnitude and varying Tu from 3 to 6% had little effect on the computed wake spreading. It is now thought that the measured wake spreading may be caused by unsteady vortex shedding from the trailing edge.

Transonic Turbine Cascade

A transonic turbine vane tested by Arts et al.[9] was also computed. Comparisons were made with measured surface pressures and heat transfer data. A C-type grid with 383 × 49 points and a wall spacing of $y^+ < 1.5$ were used. Surface heat transfer converged to plotting accuracy in 5000 iterations, which took about 8 min on the Cray C-90.

Computed distributions of isentropic surface Mach number are compared to experimental data for exit Mach numbers of 0.875 and 1.02 in Fig. 3. The B–L and k-ω models gave identical results. The subsonic results agree very well with the experimental data. The transonic results slightly underpredict the Mach number on the rear (uncovered) part of the suction surface.

Figure 4 compares measured and computed values of surface heat transfer coefficient H [W/(m^2 K)] vs distance S (mm) along the vane surface for a case with exit $M_{exit} = 0.875$, $Re_{exit} = 1 \times 10^6$, and $Tu = 4\%$. The experimental data (triangles) show laminar flow on the entire pressure surface, and on the

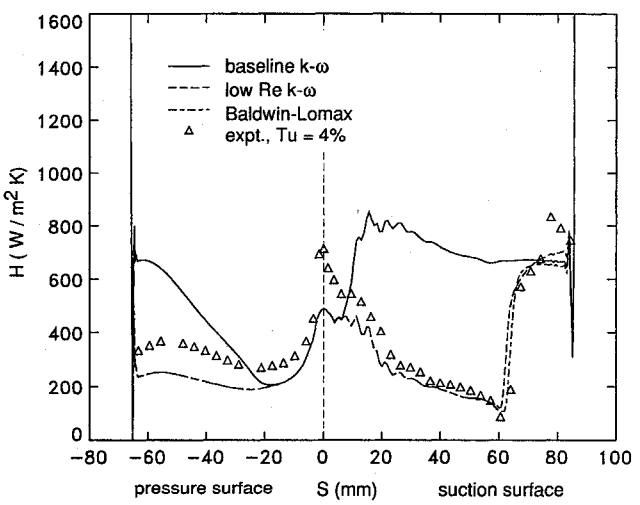

Fig. 4 Surface heat transfer coefficient predicted by three turbulence models.

suction surface up to transition at $S = 60$ mm. The laminar regions have augmented heat transfer caused by the high free-stream turbulence. This augmentation is not modeled by any of the turbulence models.

The baseline k-ω predicted fully turbulent flow on the suction surface and showed transition near $S = -20$ on the pressure surface, giving high values of H. The B–L solution agreed closely with the data using the simple transition model proposed in Ref. 1. The low Reynolds number k-ω solution also agreed closely with the data; however, the transition point was set by the choice of the inlet values of ω, as characterized by the inlet turbulent viscosity. The value of $\mu_{T,in}$ was varied by about three orders of magnitude to produce solutions that ranged from fully laminar to almost fully turbulent. Only a small range of values of $\mu_{T,in}$ gave transition near the measured location. The results shown here used $[\mu_T/\mu_{Lam}]_{in} = 7 \times 10^{-4}$. It is emphasized that although the location of transition depended strongly on $\mu_{T,in}$ or ω_{in}, the heat transfer in the fully turbulent region was nearly independent of ω_{in}.

Concluding Remarks

Wilcox's k-ω turbulence model has been added to a quasi-three-dimensional Navier–Stokes code for turbomachinery.

The model included the effects of rotation, radius change, and stream-surface convergence. An upwind-implicit approximate–factorization scheme was used to solve the turbulence model equations uncoupled from the flow equations. The numerical scheme was robust, but about 18% slower than the B–L model.

Calculations were made of a transonic compressor rotor with significant quasi-three-dimensional effects. The results showed very close agreement between the B–L and k-ω models, but both models failed to capture the measured wake spreading. Calculations were also made of a transonic turbine vane with transition and heat transfer. Both turbulence models showed very good agreement with measured surface pressures. Surface heat transfer was predicted reasonably well by the B–L model, considering the simple transition model used. The low Reynolds number k-ω model gave similar results, but the predicted transition location was sensitive to inlet values of ω. Overall the k-ω model behaved well numerically, but predictions were not decisively better than those made with the B–L model.

References

[1]Baldwin, B. S., and Lomax, H., "Thin-Layer Approximation and Algebraic Model for Separated Turbulent Flows," AIAA Paper 78-257, Jan. 1978.

[2]Wilcox, D. C., "Turbulence Modeling for CFD," DCW Industries, Inc., La Canada, CA, 1994.

[3]Wilcox, D. C., "Simulation of Transition with a Two-Equation Turbulence Model," *AIAA Journal*, Vol. 32, No. 2, 1994, pp. 247–255.

[4]Menter, F. R., "Improved Two-Equation k-ω Turbulence Model for Aerodynamic Flows," NASA TM-103975, Oct. 1992.

[5]Liu, F., and Zheng, X., "Staggered Finite Volume Scheme for Solving Cascade Flow with a k-ω Turbulence Model," *AIAA Journal*, Vol. 32, No. 8, 1994, pp. 1589–1597.

[6]Chima, R. V., "Explicit Multigrid Algorithm for Quasi-Three-Dimensional Viscous Flows in Turbomachinery," *Journal of Propulsion and Power*, Vol. 3, No. 5, 1987, pp. 397–405.

[7]Baldwin, B. S., and Barth, T. J., "A One-Equation Turbulence Transport Model for High Reynolds Number Wall-Bounded Flows," NASA TM 102847, Aug. 1990.

[8]Suder, K. L., Chima, R. V., Strazisar, A. J., and Roberts, W. B., "The Effect of Adding Thickness and Roughness to a Transonic Axial Compressor Rotor," *Journal of Turbomachinery*, Vol. 117, No. 4, 1995, pp. 491–505.

[9]Arts, T., Lambert de Rouvroit, M., and Rutherford, A. W., "Aero-Thermal Investigation of a Highly Loaded Transonic Linear Turbine Guide Vane Cascade," von Kármán Inst. for Fluid Dynamics, TN 174, Belgium, Sept. 1990.

Linear Acoustic Analysis of Solid Propellant Pressure-Coupled Distributed Combustion

Michael M. Micci*
Pennsylvania State University, University Park, Pennsylvania 16802

Nomenclature

a = speed of sound
c_p = specific heat at constant pressure
e_0 = stagnation or total internal energy
i = $\sqrt{-1}$
m_b = volumetric mass injection rate
p = pressure
R = gas constant
R_p = pressure-coupled response
R_v = velocity-coupled response
T = temperature
T_f = adiabatic flame temperature
t = time
u = gas velocity
x = distance above the propellant surface
γ = ratio of specific heats
ΔT = nonisentropic flame temperature contribution
ρ = density
ω = angular frequency

Superscripts
$'$ = perturbation quantity
$-$ = mean quantity
$\hat{}$ = complex perturbation quantity

Received Nov. 9, 1995; revision received May 6, 1996; accepted for publication June 5, 1996.

*Associate Professor, Department of Aerospace Engineering and Propulsion Engineering Research Center, 233 Hammond Building. Senior Member AIAA.

Introduction

DISTRIBUTED combustion is the term used to denote the combustion of solid particles, usually metals such as aluminum or boron, in the combustion chambers of solid propellant rocket motors after they have been emitted from the burning solid propellant surface, but before they pass through the nozzle. Beckstead[1] has shown that the unsteady particle combustion can significantly influence the rocket motor acoustic stability. Models for distributed combustion have been proposed,[2] but there currently exist no methods for experimentally measuring the unsteady distributed combustion response under conditions that simulate those found in actual solid propellant rocket motors.

However, it has been shown that in a modulated exhaust combustion chamber with solid propellant only at the head end of the chamber, in a so-called cigarette or end-burning mode, measurements of the unsteady gas velocity as functions of distance above the burning propellant surface by means of magnetic velocimetry,[3] along with measurements of the unsteady pressure, combined with a one-dimensional linear acoustic analysis of the flow within the chamber,[4] can be used to obtain the propellant pressure-coupled combustion response with a high degree of accuracy. The analysis assumed that all of the propellant combustion occurred in a region very close to the burning propellant surface, allowing the propellant response to be treated as a boundary condition. Such an assumption is valid for nonmetallized composite propellants. By modifying the acoustic analysis as described in the next section, to allow for distributed combustion away from the propellant surface, the same experimental technique can be used to measure the unsteady distributed combustion response.

Analysis

One takes the one-dimensional constant area (variable areas can be included, but are excluded here for simplicity) unsteady compressible equations for the conservation of mass, momentum, and energy with mass, momentum, and energy sources caused by the combustion of the metal particles after they are emitted from the burning solid propellant surface

$$\frac{\partial \rho}{\partial t} + \frac{\partial (\rho u)}{\partial x} = m_b \tag{1}$$

$$\frac{\partial (\rho u)}{\partial t} + \frac{\partial (\rho u^2)}{\partial x} + \frac{\partial p}{\partial x} = u m_b \tag{2}$$

$$\frac{\partial (\rho e_0)}{\partial t} + \frac{\partial (\rho u e_0)}{\partial x} + \frac{\partial (pu)}{\partial x} = c_p T_f m_b \tag{3}$$

where m_b is caused from the particle combustion.